JCTC Journal of Chemical Theory and Computation

Article

pubs.acs.org/JCTC

Work Function of Oxide Ultrathin Films on the Ag(100) Surface

Luca Sementa,[†] Giovanni Barcaro,[†] Fabio R. Negreiros,[†] Iorwerth O. Thomas,[†,▽] Falko P. Netzer,[§] Anna Maria Ferrari,[‡] and Alessandro Fortunelli*[,†]

[†]CNR-IPCF, Istituto per i Processi Chimico-Fisici of the Consiglio Nazionale delle Ricerche, Molecular Modeling Laboratory, I-56124 Pisa, Italy

[‡]Dipartimento di Chimica e IFM, Università di Torino, I-10125, Turin, Italy

[§]Surface and Interface Physics, Institute of Physics, Karl-Franzens University Graz, A-8010 Graz, Austria

Supporting Information

ABSTRACT: Theoretical calculations of the work function of monolayer (ML) and bilayer (BL) oxide films on the Ag(100) surface are reported and analyzed as a function of the nature of the oxide for first-row transition metals. The contributions due to charge compression, charge transfer and rumpling are singled out. It is found that the presence of empty d-orbitals in the oxide metal can entail a charge flow from the Ag(100) surface to the oxide film which counteracts the decrease in the work function due to charge compression. This flow can also depend on the thickness of the film and be reduced in passing from ML to BL systems. A regular trend is observed along first-row transition metals, exhibiting a maximum for CuO, in which the charge flow to the oxide is so strong as to reverse the direction of rumpling. A simple protocol to estimate separately the contribution due to charge compression is discussed, and the difference between the work function of the bare metal surface and a Pauling-like electronegativity of the free oxide slabs is used as a descriptor quantity to predict the direction of charge transfer.

1. INTRODUCTION

Ultrathin (UT) films of oxide materials, i.e., films up to a few monolayers, of thickness up to ≈1−2 nm, grown epitaxially on single-crystal metal surfaces, represent a new class of materials which has raised an increasing attention in latest years, both at a fundamental level and for potential technological applications.[1−4] Originally, the interest in these systems was motivated by the fact that, when using probes employing charged particles, the reduced thickness of oxide UT films allowed the probe particles to tunnel toward the metal support, thus making the corresponding surface science techniques applicable. Scanning tunneling microscopy (STM),[5] photoemission,[6] and other electron excitation techniques, to name a few, have been so used in the study of oxide UT films. The high level of characterization hence resulting has led to the discovery that many oxide UT films possess radically new structures and stoichiometries and that they represent a new class of materials with potentially innovative properties with respect to bulk phases.

In particular, it has been shown that the presence of an UT oxide can modulate the system work function, i.e., the energy needed to extract one electron from the system and bring it to infinity.[7−12] The work function is an important quantity which is at the basis of many interfacial phenomena, such as electronic transport, adsorption, and adhesion. Its control can lead to practical applications in many technological fields. For example, tuning the work function can reduce the contact resistance between the anode and the Hall transport layers of organic light emitting diode devices,[13] control heterogeneous catalysis in water dissociation,[14] strongly enhance field emission currents,[15] or lead to selective charging of adsorbed species, such as metal clusters.[16−18] The surface work function can be also modulated in the *xy* direction at the subnanometer level, giving rise to nanopatterned surfaces to be used for molecular self-assembly. This is the case of FeO_x UT films grown on Pt(111), where a Moiré structure is developed and the value of the work function is periodically modulated by the match between the metal and the oxide lattices.[19] Another example is given by Li doping of UT silica grown on Mo(112), where a local lowering of the work function is observed in correspondence of the sites where cationic Li are trapped.[20]

In order to elucidate the dependence of the work function on the nature of the metal/oxide pair and of the thickness/structure of the oxide deposits, first-principles theoretical approaches such as density functional (DF) ones can be profitably used. Three main effects influence the change in the system work function with respect to the bare metal surface: (i) charge compression; (ii) charge transfer between the metal and the oxide; and (iii) rumpling of the oxide layer. The delicate balance of these three quantities determines an increase or a reduction of the work function, see e.g., an analysis of simple ionic oxides grown on (100) and (111) metal surfaces in ref 21. These effects can also be entangled: as an example, in the case of MgO it has been demonstrated that rumpling effects can occur as a structural response to interfacial charge transfer.[22]

In the present paper, we use a DF approach and analyze in detail the electronic structure of a selected but representative set of metal oxide UT films, focusing initially on the NiO/Ag(100) system as a prototype of a first-row transition-metal oxide in contrast to simple ionic oxides, such as MgO, and then extending the investigation to other late first-row transition-metal oxides (MO, with M = Co, Cu, Zn). The contributions to the system work function due to charge compression, charge

Received: October 3, 2011
Published: January 4, 2012

   dx.doi.org/10.1021/ct200861f | J. Chem. TheoryComput. 2012, 8, 629−638

transfer, and rumpling are disentangled and estimated as a function of the thickness of the film. A method to evaluate the contribution due to charge compression is proposed, and a Pauling-like electronegativity is used as a descriptor to predict the direction of charge transfer. This analysis reveals a more varied and interesting panorama than what has been previously assumed in the literature especially focused on the case of simple ionic oxides, as in the case of transition metals, the mixed covalent/ionic nature of the oxidic bond plays a fundamental role. Depending on the specific system combination, charge transfer and rumpling can drive an increase or a decrease of the work function and can operate synergistically or in opposite directions. For example, for NiO, an oscillating behavior of the system work function as a function of the oxide thickness is found and rationalized, while in CuO, charge-transfer effects are so large that an inverse rumpling occurs and, interestingly, a CuO bilayer (BL) on Ag(100) is predicted to exhibit a work function larger than that of the metal surface.

The article is organized as follows: In Section 2 the theoretical methods are described in detail. Results are presented and discussed in Section 3, while Section 4 summarizes the main conclusions.

2. THEORETICAL METHODS

The present calculations were performed on periodic slab models using the QuantumEspresso (QE) package[23] and CRYSTAL09[24,25] periodic codes, employing DF theory with gradient-corrected or hybrid exchange−correlation (xc-) functionals. QE calculations employ a basis set of plane waves, ultrasoft pseudopotentials,[26] and the Perdew−Burke−Ernzerhof (PBE) xc-functional.[27] Spin-polarized calculations were performed by applying a pure DF approach or a DF+U approach;[28] in the latter case, the value for the Hubbard term (U) on the d-orbitals of the metal species was chosen in the range between 0 and 5.3 eV, as detailed in the following. In selected calculations, larger values of U for the oxide metals and a Hubbard term on the 2p-orbitals of the O atoms were used to damp the charge transfer from the metal and achieve a separate estimate of this effect. In the literature, the value of the U term is usually fixed it by comparison with experimental data or other first-principles calculations. For the bulk system, the U value is chosen in such a way as to reproduce the band gap. For an ultrathin film, screening effects in general reduce the value of U for the metal atoms at the interface with respect to the bulk, by roughly 1.3−2.0 eV on the Ag(100) support, as shown by experimental[29,30] and theoretical[31] estimates. The U values used in the present work have been selected via this approach, i.e., by reducing by ≈2 eV the values appropriate for the bulk.[32] Values of 40 and 160 Ry were chosen as the energy cutoff for the selection of the plane waves for the description of the wave function and the electronic density, respectively. The first Brillouin zone was k-sampled by employing a (4,4,1) grid, and the electronic levels were broadened with a Gaussian smearing of about 0.03 eV. CRYSTAL09 calculations were performed using a hybrid DF xc-functional and a localized basis set of Gaussian-type functions (GTF). The basis set used in present calculations consists of: relativistic small core pseudopotentials[33] (19 electrons) together with 4s4p2d contracted GTF for Ag8-411G(d) functions for O ions; 8-511G for Mg; and 6sp2d GTF for Co, Ni, Cu and Zn.[34] The standard Becke hybrid-exchange xc-functional,[35] with 20% of exact Fock exchange together with a Perdew−Wang correlation functional[36] (B3PW91), accounts for the localized nature of the unpaired electrons in magnetic systems[37,38] and has been shown to adequately describe the electronic and magnetic structures of many metal oxides. Especially bulk band gaps are often more accurately predicted by a hybrid xc-functional,[32] in particular if one uses (which however is not the case here) the so-called range-separated or screened ones.[39] A Fermi−Dirac finite smearing broadening of 0.01 au has been adopted in all calculations. In both computational approaches (QE and CRYSTAL), the metal support was described using five Ag layers in (100) stacking and considering a symmetric adsorption of oxide films on both sides of the metallic slab (to cancel the total dipole moment of the system). This thickness of the metal slab is sufficient to provide converged values: work functions were validated in selected cases to be practically coincident with those obtained using seven or more layers. The atoms of the innermost three layers were kept fixed in the positions of bulk fcc crystal (with a first-neighbor distance of 2.89 Å, corresponding to the experimental value for bulk silver), whereas the positions of the outer layers on each side, as well as the coordinates of the oxide atoms, were fully optimized until the forces were smaller than 0.01 eV/Å per atom (QE) or 0.00045 au (CRYSTAL). In general, the behavior of the work function does not change if performing calculations at the DF-optimized Ag bulk lattice parameter. In QE calculations a minimum empty space of 10 Å was chosen along the z axis of the 3D cell to avoid interactions between replicated cells, whereas 2D periodic slab models, characterized by two infinite dimensions (x and y) and a finite thickness, were employed in CRYSTAL calculations. In the case of magnetic systems, an antiferromagnetic AFM2 arrangement of the spins on the metal atoms was considered.

The work function was calculated in a standard way as the difference between the vacuum level of the potential and the Fermi energy of the system. In QE, due to the replicated character of the model, one has to ensure that enough vacuum is left between replicated slabs so that the potential stabilizes to a constant value (plateau). This is not necessary in CRYSTAL, based on a real 2D modeling. However, work function values are extremely sensitive to set basis incompleteness when adopting localized GTF in CRYSTAL calculations. A useful expedient to overcome the basis set limitations is to employ an array of ghost functions localized at a proper distance from the surface.[40] In the present calculations a regular array of s-like GTF (with exponent α =1.0) located at a distance d = 2.0 Å from the surface was adopted in all calculations. For instance, the calculated Ag work function changes from 2.5 eV (without ghost array) to 4.22 eV (by adding the ghost array), the latter value being in excellent agreement with the corresponding experimental data (4.22 eV).[41]

Finally, charges were usually estimated using a Lowdin projection onto an atomic basis set in the QE approach, with the exception of those reported in Table 1 to evaluate accurately the interfacial charge transfer: these were obtained using a Bader analysis[42] as implemented in the ABINIT code by K. Casek, F. Finocchi, and X. Gonze. Lowdin charges, derived from a projection onto an incomplete basis set in the QE approach, do not equal the total number of electrons. However, their differences are meaningful as they usually parallel those obtained via more sophisticated approaches, such as the Bader one, and are thus reported below to highlight semiquantitative trends.

Table 1. Interfacial Charge Transfer per MO Unit for Different Oxide ML Films [M = Mg, Co, Ni, Cu, Zn] deposited on the Ag(100) Surface[a]

MgO	NiO (U large)	CoO	NiO (rumpled)	NiO	CuO	ZnO
−0.078	+0.011	+0.033	+0.079	+0.099	+0.143	+0.034

[a]Flat geometries are used, except for the NiO (rumpled) system, which corresponds to the fully relaxed NiO/Ag(100) ML. A U value of 4 eV is used, except for Mg, for which U = 0, and NiO (U large), for which U = 16 eV, is used on Ni and U = 12 eV for O, respectively. Charges are calculated according the Bader scheme. Positive values indicate transfer of electrons from the Ag support to the oxide film.

3. RESULTS AND DISCUSSION

We start by discussing the case of NiO as a prototypical example of first-row transition-metal oxide. Bulk NiO is characterized by a rock-salt structure with an experimental lattice constant of 4.16 Å and a band gap between 4.0 and 4.3 eV. At the DF+U/PBE level, choosing a proper value for the Hubbard term (U = 5.3 eV), the equilibrium lattice constant is 4.22 Å, and the difference between the highest occupied molecular orbital (HOMO) and the lowest unoccupied molecular orbital (LUMO) amounts to 2.96 eV. In an unsupported NiO monolayer (ML) at this level of theory, the equilibrium distance between first-neighbors oxygen atoms is equal to 2.80 Å. This value increases to 2.90 Å when the oxide ML is adsorbed on Ag(100), due to the interaction with the metal support.[31] When considering NiO deposited on silver surfaces, the U value has been reduced from 5.3 to 4.0 eV to take into account screening by the metal support, as discussed in refs 29−31.

The equilibrium value of the lattice parameter of the NiO adsorbed ML is close to the lattice constant of the Ag(100) surface, entailing that an almost perfect pseudomorphic growth is favored: the O atoms of the oxide are adsorbed on top of the silver atoms, whereas the nickel atoms fall in hollow sites of the metal surface (see Figure 1a). From the values in Figure 1b, where equilibrium geometrical parameters of the oxide slabs are reported, it can be seen that the oxide ML presents a small rumpling, with the Ni atoms slightly closer to the surface plane (on average by 0.15 Å) than the oxygen atoms. When growing further oxide layers, the average height of the first layer increases but is still characterized by a similar rumpling.

Figure 1c shows the values of the system work function as a function of the thickness of the oxide film, both in the case of flat and rumpled oxide films. It should be noted that in the case of flat films, we chose a common height corresponding to the average between the optimized heights of the cations and of the anions. A comparison of the two curves shows that the same qualitative behavior is found. The first oxide layer increases the work function of the silver surface, whereas deposition of further layers produces a decrease. To rationalize this behavior, we need to partition the work function into different contributions.

As discussed, e.g., in ref 22, in the case of MgO on a variety of metal surfaces, the value of the system work function depends on the electric dipole developed at the surface. When an oxide layer is adsorbed on the metal substrate, three effects affect the value of this surface dipole: (i) charge compression; (ii) charge transfer between the metal and the oxide; and (iii) rumpling of the oxide layer. Charge compression, i.e., the repulsion exerted by the electron cloud of the oxide on the

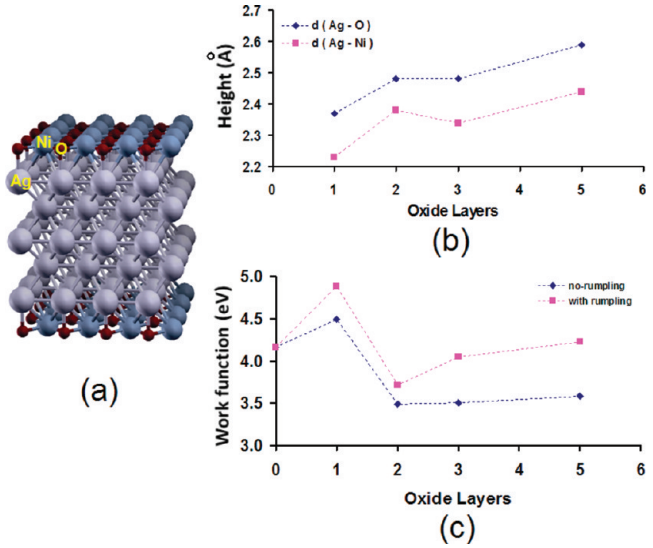

Figure 1. (a) Schematic picture of an Ag(100) slab terminated on both sides by a NiO ML; (b) equilibrium height above the silver surface of the Ni (pink squares) and O (blue diamonds) atoms of the oxide layer in contact with the metallic slab as a function of the thickness of the oxide film; and (c) work function of the system as a function of the oxide thickness, both in the case of a rumpled (pink squares) or flat (blue diamonds) oxide. Results from from DF+U/PBE calculations using U_{Ni} = 5.3 eV, except for the Ni atoms at the interface for which U_{Ni} = 4 eV.

electrons on the metal surface, decreases the value of the work function, as the metal electrons are pushed back into the surface with a consequent decrease of the net surface dipole. Charge transfer and rumpling effects instead can determine an increase or a decrease of the work function, depending on the nature of the metal surface and the oxide. For example, when MgO is adsorbed on Ag(100), the silver surface gets a negative charge (due to a charge transfer from the O atoms to the metal surface) determining a decrease of the work function, see e.g., ref 17. As a consequence, the Mg cations are attracted by the negatively charged silver surface, and the rumpling dipole moment developed in this way determines an increase of the work function. It has been observed[22] that in the case of MgO, the effects of charge transfer and rumpling always work in opposite directions. The case of transition metal oxides, such as NiO, is more complicated, as it will be illustrated presently.

To begin with, let us consider flat films, so that rumpling makes no contribution to the work function. In the case of a ML, the value of the work function (4.4 eV) is increased with respect to the pure (100) silver surface (4.1 eV). As the effect of the charge compression is to decrease the work function, charge transfer must play a role. This is confirmed by the inspection the charge density difference shown in Figure 2a, where the difference between the electronic density of the NiO/Ag(100) system and that of the two isolated fragments—bare Ag(100) surface and unsupported NiO ML—is plotted.[43] In the composite system, electronic density flows from the silver surface to the Ni atoms of the oxide layer. To disentangle charge-transfer and charge compression contributions, we performed a single point calculation where large values of the Hubbard U term were put on both Ni and O atoms (specifically, U = 16 eV on Ni and U = 12 eV on O). Following this strategy, the charge flow from the silver surface to the oxide is strongly reduced (see Figure 2b). The value of

dx.doi.org/10.1021/ct200861f | J. Chem. TheoryComput. 2012, 8, 629−638

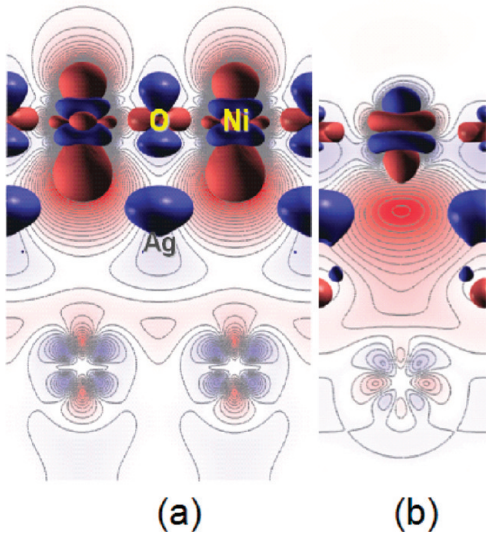

Figure 2. (a) Electron density difference between the NiO-ML/Ag(100) system and the two isolated fragments, bare Ag(100) surface and unsupported NiO ML from DF+U/PBE calculations using U_{Ni} = 4 eV; (b) same plot obtained by using U = 16 eV on Ni and U = 12 eV on O. A dark-blue color represents a depletion of electron density, a light-red color an increase.

the work function in this case amounts to 3.2 eV and essentially corresponds to a pure charge compression effect, which at this geometry is found to determine a decrease of the work function of about 0.9 eV. We thus estimate that charge transfer taken individually produces an increase of the work function of the ML of about 1.2 eV. The trick of using large U values on both the metal and the oxygen atoms of the oxide to annihilate charge-transfer effects and estimate a pure charge compression contribution is a convenient tool to make a quantitative analysis. To further support this contention, in Figure S1, Supporting Information, we report the behavior of the work function of the NiO/Ag(100) ML system as a function of the value of Hubbard U used on the Ni atoms (a qualitatively similar plot is obtained if the U value on the O atoms is used as independent variable but with a much smaller excursion). As apparent from this figure, the proposed approach is relatively insensitive to the precise value of the Hubbard U, once the plateau region is reached.

Adding now the rumpling contribution, we see that this goes in the same direction as that from charge transfer (at variance with the MgO case[22]), as rumpling also produces an increase in the system work function from 4.4 to 4.8 eV (see Figure 1c). The main difference between MgO and NiO is that in MgO the physics of the system is mainly driven by electrostatic effects. On the contrary, NiO presents low-energy empty orbitals (the d orbitals on Ni cations) which can accommodate electron density from the surface and orient the rumpling of the oxide in such a way that the two dipoles (the one originating from charge transfer and the one from rumpling) go in the same direction.

To further substantiate the proposed analysis of the charge transfer, we report in Table 1 the values of interfacial charge transfer between the Ag support and the NiO film (other oxide films are also reported in Table 1, to be discussed below) obtained via an accurate (although computationally expensive) Bader analysis of the wave function.[42] In the case of a NiO flat ML, Ag(100) yields about 0.1 electrons to the oxide, but using large values of U on both Ni and O atoms effectively quenches this charge transfer by an order of magnitude, confirming the usefulness of this approach. It can also be noted from Table 1

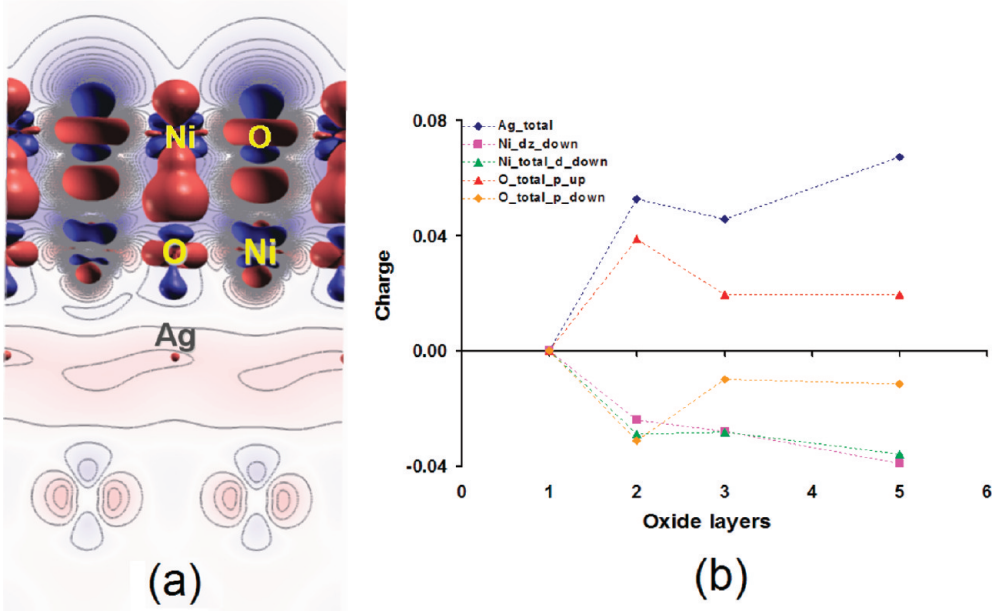

Figure 3. (a) Difference between the electronic density of the NiO-BL/Ag(100) system and that of the two isolated fragments: NiO ML/Ag(100) and unsupported NiO ML; (b) Lowdin charge differences as a function of the number of oxide layers: As a reference point, the net charge on Ni, O, and Ag atoms are set equal to 0 in the case of the system NiO ML/Ag(100). The values of the Lowdin total charges are: 8.92 (Ni), 7.06 (O), and 10.77 (Ag at the interface), with 10.95 the topmost Ag atom in a bare Ag(100) surface and 8.69 (Ni) and 7.12 (O) in a gas-phase NiO ML. From top to bottom: Ag at the interface total (blue diamonds), O total 2p spin up (red triangles), O total 2p spin down, Ni d_{z2} spin down (pink squares), and Ni total d spin down (green triangles). Reported results are from DF+U/PBE calculations using U_{Ni} = 5.3 eV, except for the Ni atoms at the interface for which U_{Ni} = 4 eV. Color coding as in Figure 2.

dx.doi.org/10.1021/ct200861f | J. Chem. TheoryComput. 2012, 8, 629–638

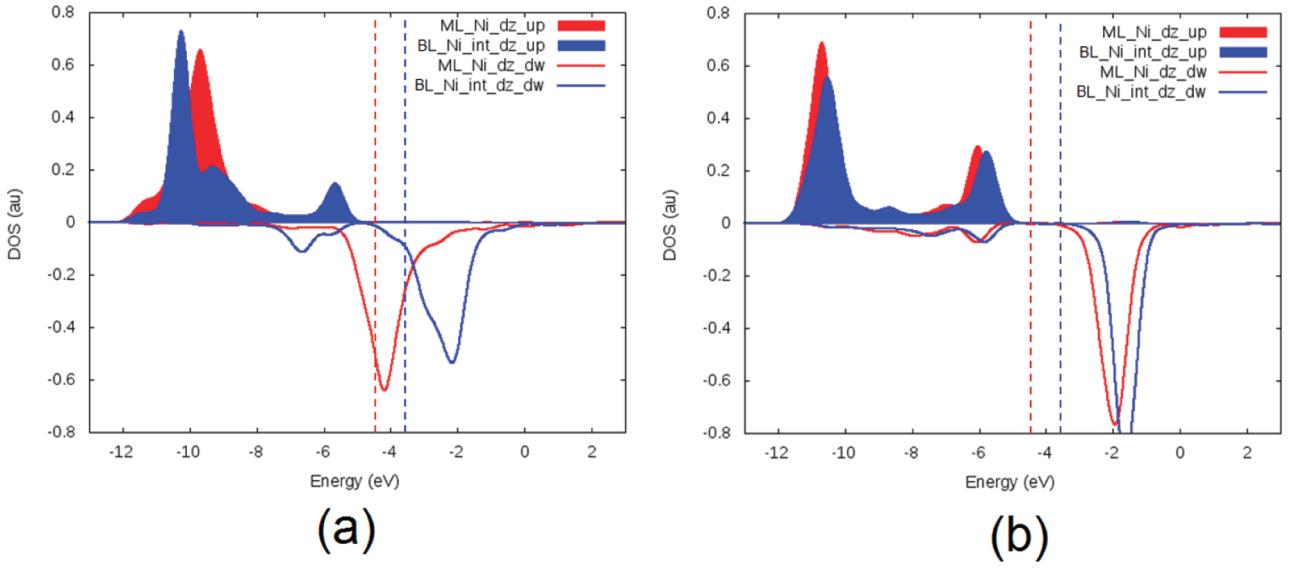

Figure 4. PDOS showing how the d_{z2} (a) and d_{x2-y2} (b) population on a Ni atom of the first layer are affected when passing from the ML to the BL system. Results from from DF+U/PBE calculations using U_{Ni} = 5.3 eV, except for the Ni atoms at the interface for which U_{Ni} = 4 eV.

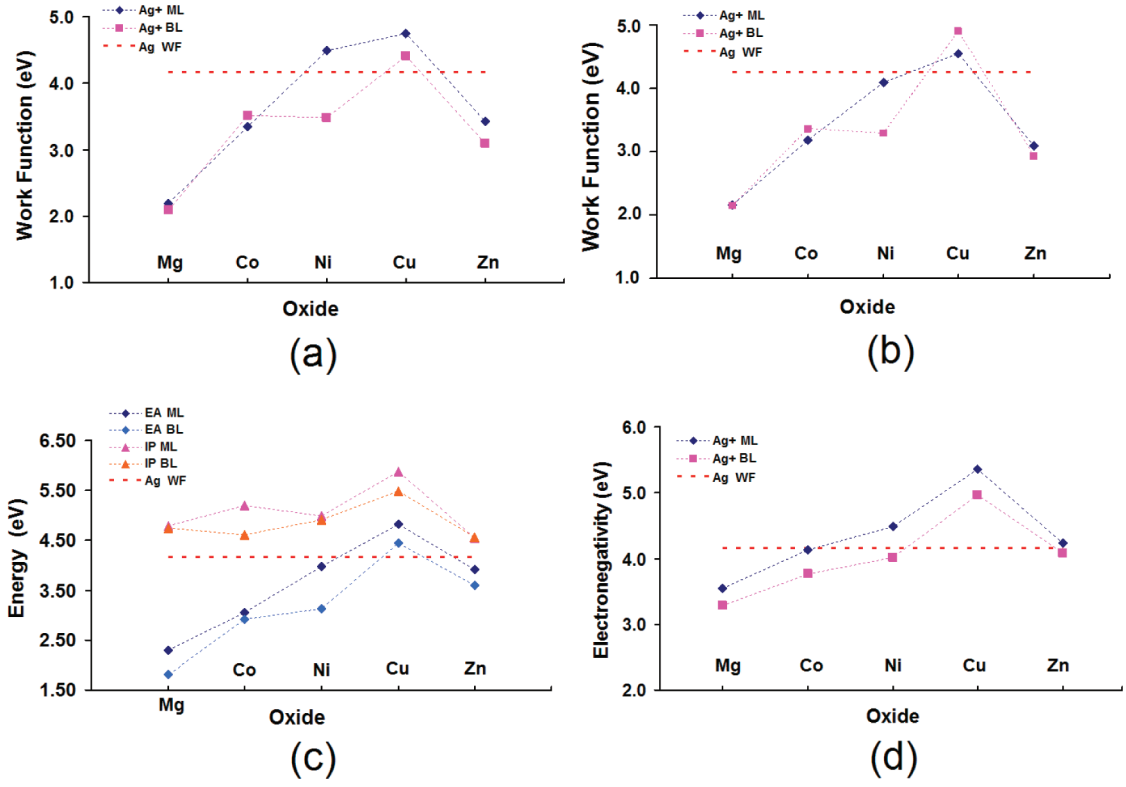

Figure 5. Values of the work function (a,b), ionization potential and electron affinities (c), and electronegativity (d) in the case of ultrathin oxides adsorbed on Ag(100). The value of the work function of Ag(100) is shown as a dotted line. In (a,c,d) quantities are calculated using a DF+U/PBE approach as implemented in the QE software using U = 5.3 eV for the metal atoms in the top oxide layer and U = 4 eV for the metal atoms at the interface, whereas in (b) work functions are calculated using a B3PW91 approach using GTF as implemented in the CRYSYAL09 software. In all cases, flat geometries obtained at the DF+U/PBE levels are employed.

that the increase in the surface dipole moment due to rumpling in NiO ML is accompanied by a decrease of the charge transfer from the support to the oxide film: One finds a reduction of ≈20% (roughly from 0.1 to 0.08 electrons) in the interfacial charge transfer after rumpling, see in Table 1 "NiO rumpled" vs (flat) "NiO".

Summarizing the results on the NiO ML, we find that the charge compression decreases the work function from 4.1 to 3.2 eV, whereas charge transfer and rumpling increase the work function to 4.4 eV (without rumpling) or 4.8 eV (with rumpling).

Let us now consider a NiO BL. As it can be seen in Figure 1c, the value of the work function in the case of BL adsorption is

dx.doi.org/10.1021/ct200861f | J. Chem. TheoryComput. 2012, 8, 629–638

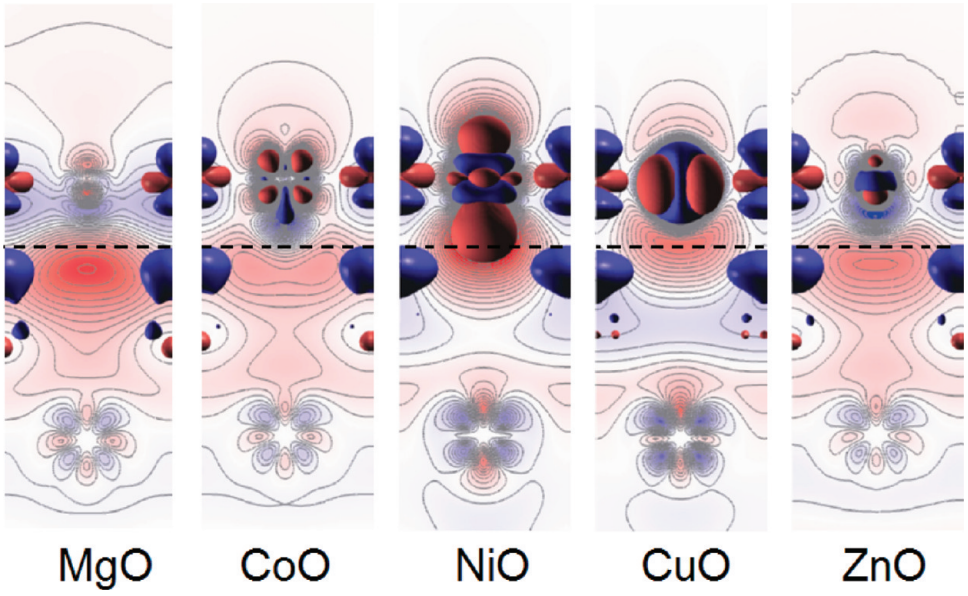

Figure 6. Difference between the electronic density of the oxide ML/Ag(100) system and that of the two isolated fragments, bare Ag(100) surface and unsupported oxide (MO) ML with M = Mg, Co, Ni, Cu, Zn. The black dashed line is located at middle average between the metal surface and the oxide layer. Color coding as in Figure 2. Results of DF+U/PBE calculations using U = 5.3 eV for the metal atoms in the top oxide layer and U = 4 eV for the metal atoms at the interface.

about 3.5 eV. In a first approximation, we can assume that the decrease caused by the charge compression is roughly the same as in the case of the ML, as it is the oxide layer in contact with the silver surface that compress the metal electronic density, and its distance from the surface is similar. We thus expect a decrease in the work function due to this effect to roughly 3.2 eV. From Figure 1c, we see that, in absence of oxide rumpling, the charge transfer determines an increase of about 0.3 eV, a value much smaller than in the case of the ML. The analysis of the charge transfer can help us to elucidate this phenomenon. By comparing the ML with the BL as done in Figure 3a, one can immediately see that the electronic density is increased on the silver surface and decreased on the Ni atoms. An analysis of the Lowdin charges (whose differences with respect to the ML case are reported in Figure 3b) further confirms this interpretation: the total charge on the Ag surface atoms increases by thickening the oxide film. Thickening of the oxide layer is thus accompanied by a partial reversal of the charge flow or a decrease in the charge-transfer dipole moment. Analyzing Figure 3a,b in more detail, we see that most of the charge lost by the Ni atoms has left the d_{z2} orbital associated with the minority spin. This point is further confirmed by a plot of the projected density of states (PDOS) reported in Figure 4, which shows how the minority spin component of the d_{z2} orbital is depleted in the BL system, in the sense that in the ML, this orbital is centered around the Fermi level, whereas in the BL, it lies above it and is thus basically unoccupied; the d_{x2-y2} orbital is much less affected. This is a crystal field effect, as the d_{z2} orbital on a Ni cation of the first layer is strongly destabilized when a negative O atom of the second oxide layer is adsorbed on top of it: due to electrostatic repulsion, the extra electrons on the Ni atoms of the first layer are pushed back into the silver substrate. The back migration of charge toward the silver surface is apparent in Figure 3a, where we observe a diffuse cloud of increased electron density in the region of the metallic surface and by the values of the atomic Lowdin charges plotted in Figure 3b.

The changes in the system work function can thus be rationalized in terms of the different contributions to the electric surface dipole for ultrathin films of NiO on Ag(100), with charge compression estimated by tuning the U values and rumpling by tuning the geometry.

An interesting question is whether it is possible to define a descriptor able to predict the direction of the charge transfer between the oxide and the metal support. In order to answer this question, we have extended our analysis to other oxide films formed by first-row transition metals adsorbed on Ag(100). To disentangle electronic and geometric degrees of freedom (we recall that charge compression is also dependent on the geometry), we have taken the flat structures obtained for the NiO slabs and substituted the Ni atoms with other metals, specifically Mg, Co, Cu, and Zn. In a first step also the U values were kept constant and equal to 4.0 eV on the metallic species of the different oxides (i.e., the value appropriate for NiO), with the only exception of MgO where we used U = 0 on Mg. These U values are not unrealistic as Co, Cu, and Zn are close to Ni in the periodic table, more precise U values for these elements will be used in the following. The values of the work function so obtained corresponding to ML and BL systems on Ag(100) are shown in Figure 5a. In most cases (with the exception of NiO), the values of the work function are similar for the ML and the BL systems. In some cases (MgO, CoO, and ZnO) these values are smaller than the work function of the bare metal surface. For CuO the values are larger, while in the case of NiO the value for the ML is larger, whereas the value for the BL is smaller. The charge flow in these systems is further visualized in Figure 6, where plots of electron density differences between the composite system and the interacting fragments (as always the U values on the fragments are those appropriate for the adsorbed layers) are shown.

To further validate these results, we have repeated the calculations with a substantially different approach, employing a GTF basis set and a hybrid B3PW91 xc-functional, as implemented in the CRYSTAL09 package. The results are

dx.doi.org/10.1021/ct200861f | J. Chem. TheoryComput. 2012, 8, 629–638

shown in Figure 5b, where the geometries are again those obtained for flat geometries at the DF+U/PBE level so that we do not introduce too many degrees of freedom at the same time. We underline that a (100)/(100) epitaxy is not unrealistic for the investigated oxides: CuO is monoclinic in the bulk, but as a ML, it is likely to be similar to NiO, while ZnO exhibits a graphitic essentially flat structure on Pd(111) and Ag(111) rather than a wurzitic one which is only obtained as the thickness of the film increases toward the bulk.[44] By comparing the two plots 5a and 5b, one can find the same qualitative behavior. From a quantitative point of view, some differences can be highlighted for NiO and CuO. In the former case, the GTF approach predicts a work function of the ML slightly smaller than that of the bare silver surface; in the latter case, the GTF approach predicts a slight increase in the value of the work function when passing from the ML to the BL system (opposite to the slight decrease predicted by the QE approach). These slight discrepancies, which are due to nonoptimal U values on the metal cations, do not affect our main conclusions.

To rationalize these numbers, we recall that charge compression always determines a decrease of the work function, which should be roughly similar for the cases here considered as all the systems share the same geometry, whereas the charge transfer (rumpling has been eliminated by focusing on flat geometries) depends on the specific ability of the oxide to receive/donate electronic density. Such an ability for simple systems is usually interpreted in terms of a Pauling-like electronegativity[45] defined as the arithmetic average between the first ionization potential and the electronic affinity of the atom. When dealing with a solid-state system (characterized by a band structure), the rough analogues of ionization potential and electronic affinity can be defined as

$$\mathrm{IP} = E_{\mathrm{vacuum}} - E_{\mathrm{maximum(VB)}}$$

$$\mathrm{EA} = E_{\mathrm{vacuum}} - E_{\mathrm{bottom(CB)}}$$

where $E_{\mathrm{maximum(VB)}}$ and $E_{\mathrm{bottom(CB)}}$ correspond to the energy at the top of the valence band and at the bottom of the conduction band, respectively, and E_{vacuum} is the energy of the vacuum level. To estimate the direction of charge transfer, one can then compare the electronegativity of the oxide slab with the work function of the bare metal support. This comparison coincides with the analysis of the position of the Fermi level with respect to the band gap of the oxide slab, a quantity traditionally employed to discuss, e.g., Schottky barriers between a metal and an insulator.[46,47,22,48] The center of the band gap of the oxide film in this approach represents a "zero charge point", i.e., deviation of the metal work function from this point induces a net charge[49,50] which correlates with interface Fermi level.[51] For the oxides considered in this work, the values of IPs and EAs are shown in Figure 5c, while the corresponding values of the Pauling electronegativity are shown in Figure 5d. From a comparison of Figure 5a,d, we see that the electronegativity values correlate well with the work function values both qualitatively and semiquantitatively. It should be noted that the values of the work function should be shifted upward because of the reduction due to charge compression, thus making the correlation even more precise.

The reasons of a decreased/increased value of the work function with respect to the pure silver surface associated with charge transfer can be clearly understood by inspecting plots of electron density differences shown in Figure 6. In the case of MgO, the main effect is due to charge compression plus a charge transfer from the oxide to the metal, which explains the reduction of the work function with respect to the pure silver surface; in this oxide the Mg^{2+} cation is not involved in any charge back donation. The situation is somewhat similar for ZnO, where the Zn^{2+} cations present an inert d^{10} closed shell configuration, but in this case, the charge transfer between oxide ML and metal is very little (from the electronegativity value we know that it is in the opposite direction with respect to MgO: from the metal to the oxide) so that the reduction in the work function is mostly due to charge compression. In the case of the other three transition-metal oxides (CoO, NiO, and CuO), there are empty d metal orbitals able to accommodate electronic density coming from the metal surface. Nevertheless, in the case of CoO, it is evident that a very small charge transfer exists, again in agreement with the small difference between the electronegativity of a free CoO ML and the work function of the bare metal. CoO is thus similar to ZnO both in terms of electron density (see Figure 6) and work function (see Figure 5a). It is interesting to underline in this connection that the vaues of the work function for CoO and ZnO (around 3.4 eV), which are the systems in which charge transfer is small, are close to that obtained for NiO by setting large values of U on both Ni and O (3.2 eV). This further validates the approach of using large values of U on both the metal and oxygen atoms of the oxide slab to annihilate charge transfer and evaluate separately the effect of charge compression. Note in fact the similarity of Figure 2a with Figure 6 for CoO and ZnO. In the case of the other two oxides (those indeed characterized by a work function of the ML larger than that of pure silver), a net charge flow from silver to the metal cations takes place. This is particularly strong in the case of CuO (see the blue region in the silver layer for this oxide), which has the largest value of the work function. This charge transfer is so high that the Ag support becomes positively charged to a degree large enough to produce a (small) inverted rumpling; the oxygen anions get closer to the surface than the Cu cations. In this phenomenon, which is peculiar to CuO, the surface dipole due to rumpling is opposite to that due to charge transfer, in analogy to the MgO case.[22] The quantitative details of this effect however are not easy to predict accurately as confirmed by the discrepancies between QE and CRYSTAL results in Figure 5a,b. It can be noted anyway that, despite these differences, CuO is the only case from both approaches in which the work function of the BL system is higher than that of the bare surface.

To validate the above analysis, the interfacial charge transfer has been accurately evaluated using a Bader analysis of the wave function.[42] The values of the charge transfer between the Ag support and the oxide ML films considered in Figure 6 are reported in Table 1. These values fully confirm that MgO yields charge to the support, whereas NiO and CuO acquire electron charge. CoO and ZnO are confirmed to be slightly electron acceptors, and we recall the above observation that the model NiO system with large values of U on both Ni and O has the smallest (and practically negligible) absolute value of charge transfer, lending further support to the proposed protocol to estimate pure charge compression effects.

At this point it is interesting to provide quantitative predictions also for the oxides other than NiO. We have thus considered the same ML oxide films as before via a DF+U approach (QE code) but now using realistic values of U on the metal atoms and allowing a full structural relaxation. As discussed in Section 2, the U values are those appropriate for the bulk phases[32] but reduced by ≈2 eV to take into account

interfacial screening effects, so that the final values employed are: U = 0, 1, 4, 2, and 6 eV for Mg, Co, Ni, Cu, and Zn, respectively. The resulting values of the work function are reported in Figure 7. An inspection of this figure shows that the

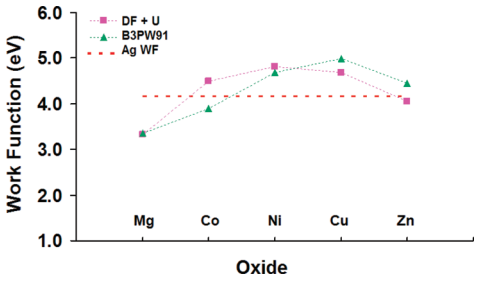

Figure 7. Values of the work function for ultrathin oxide ML films adsorbed on Ag(100) according to DF+U (QE code) and B3PW91 (CRYSTAL code) approaches. The value of the work function of Ag(100) is shown as a dotted line. The geometry is fully relaxed in all cases.

qualitative trend found for the previously considered model systems still remains after a precise and quantitative modeling. Minor differences are due to the fact that rumpling increases the work function, especially for the CoO and ZnO systems. In Figure 7 the values obtained considering a full structural relaxation also via the B3PW91 approach are also reported. A fundamental consistency between DF+U and hybrid approaches is again apparent, which further supports our analysis and predictions.

So far we have focused on the Ag(100) surface and on (100)/(100) epitaxy, i.e., oxide slabs with rock-salt structure cut along a (100) facet and deposited on the Ag(100) surface with O atoms eclipsing Ag ones. We conclude our presentation by showing that the concepts previously introduced are helpful to rationalize the behavior of systems quite different from those so far considered. In particular, we will consider (111)/(111) pseudoepitaxial systems, which are ubiquitous in oxide ultrathin films and present both a scientific and a technological interest. The first major difference we expect with respect to (100)/(100) epitaxy is in the contribution to the work function due to charge compression, which depends on the details of the epitaxial relationships between the oxide film and the metal support. Furthermore, at variance with (100) substrates in which nonpolar phases are abundant, *polar* phases are a very common occurrence on (111) substrates, see refs 52 and 22 and references therein. For these phases the rumpling contribution can assume a much greater importance than for (100) nonpolar films and become crucial in determining the values of the work function. Even though other structures are possible,[22] in many of these polar phases one often finds the metal atoms of the oxide at the interface in fcc hollow sites of the (111) surface and an oxygen overlayer appreciably further from the support in hcp hollow sites to realize an ABC stacking,[52] i.e., one does not have eclipsing of support and oxide atoms as in (100)/(100) epitaxy. In such cases, the charge compression will be much reduced with respect to the cases considered for (100)/(100) epitaxy in which the oxygen atoms were positioned on top of the metal atoms of the support, and one will likely pass from large charge-compression/small rumpling to small charge-compression/large rumpling systems.

For example, in ref 53 a titanium oxide ML grown on the Pt(111) surface was investigated. This is a polar system, i.e., it exhibits a strong rumpling with a Ti layer positioned at about 2.15 Å and an O overlayer positioned at about 2.90 Å above the Pt(111) surface. The dipole moment across the surface is 1.84 au. It must be stressed that, although the atomic stacking is Pt−Ti^{+}−O^{-}, the direction of this dipole moment is such that its negative pole is on the metal slab and the positive one on the oxide slab. This counterintuitive result is due to the fact that the TiO_x slab donates electron charge to Pt(111). This could be expected as titanium is at the beginning of the transition row (i.e., titanium oxide slabs should have a low electronegativity from an extrapolation of the plot in Figure 5) and that the work function of Pt(111) is much higher that that of Ag(100), about 5.6 eV. Despite this substantial charge transfer, the work function of this system is only slightly reduced with respect to that of the bare Pt(111) surface.[31] Charge compression effects are in fact much smaller for (111) than for (100) epitaxy. In the ideal (111)/(111) epitaxy with fcc stacking, titanium cations are adsorbed in hollow sites of the surface, and oxygen anions are also adsorbed in hollow sites of and much further from the surface (due to rumpling) instead of being located on top of surface metals. As rationalized for ZnO/Ag(111) below, in this case charge compression is small. The game is thus between charge transfer to the metal and the polarity of the slab. It turns out that these two effects nearly compensate for TiO_x reduced ML on Pt(111) so that the system work function finally results only slightly decreased with respect to that of the bare surface. Analogous cases[20,54] can be treated similarly.

As another example, a graphitic-like ZnO ML grown on Ag(111) was found to exhibit a work function slightly increased (by 0.3 eV) with respect to the bare Ag(111) surface.[31] In this case, a flat ZnO film lies at an average height of 2.82 Å from the Ag surface, while an average height difference of ≈0.1 Å between Zn and O atoms is produced when the film is allowed to rumple. We know from Figure 5 that a (100) ZnO ML has an electronegativity very close to that of Ag(100), and we recall that the work function of Ag(100) and Ag(111) is very similar (i.e., 4.1 and 4.2 eV, respectively, from our theoretical QE approach). In detail, the electronegativity of a ZnO(111) ML in the gas phase is 4.25 eV, thus slightly larger than the work function of Ag(111), and a charge transfer from the support to the oxide is expected, although small. However, charge compression effects are much smaller for (111) epitaxy. To achieve a quantitative estimate, we used the same procedure employed for NiO on Ag(100): (i) First we considered a flat ML in which the Zn and O atoms were positioned at an average height; (ii) we used large U values on both Zn and O (16 and 12 eV, respectively) to estimate separately the effect of charge compression (and thus indirectly that of charge transfer); and (iii) we fully relaxed the system to quantify the effect of rumpling. It turned out that charge compression in this case decreases the work function by only −0.01 eV, an effect which is compensated by charge transfer from Ag(111) to ZnO which eventually produces an increase in the work function by +0.05 eV. Finally, rumpling further increases the work function by 0.25 eV. As expected from the considerations outlined above, for (111)/(111) epitaxial systems, charge compression can thus play a lesser role with respect to charge transfer and rumpling.

4. CONCLUSIONS

The work function of metal surfaces covered with oxide films, i.e., the work needed to extract one electron from the system and bring it to infinity, is an important quantity which is at the basis of many interfacial phenomena, such as electronic

transport, adsorption, and adhesion. In the present article, the work function of oxide ultrathin films on the Ag(100) surface is analyzed in detail to disentangle its three contributions: charge compression, charge transfer, and rumpling, as a function of the nature of the oxide and the thickness of the film. This analysis reveals a more varied panorama than previously assumed. Depending on the specific system combination, charge transfer and rumpling can drive an increase or a decrease of the work function and can operate synergistically or in opposite directions. With respect to simple ionics, such as MgO, the presence of empty d orbitals in transition-metal oxides can entail a charge flow from the Ag(100) surface to the oxide film and thus a partial or more than full recovery of the reduction in the work function due to charge compression. This peaks for CuO, the only system here considered in which the BL has a work function larger than that of the bare surface and which presents a rumpling with the oxygen anions closer to the surface than the counter-cations. With the aim of deriving some general principles in addition to depicting a phenomenology which can serve as a framework for future studies, the effects of charge compression, charge transfer, and rumpling are analyzed separately via a 'gedanken-experiment' in which (i) one starts from the separated oxide and metal fragments; then (ii) lets them approach at the equilibrium distance simultaneously constraining the oxide film and the metal to keep a flat configuration; (iii) changes the nature of the oxide by keeping the geometry frozen to estimate the contributions due to charge compression and charge transfer separately; and finally (iv) allows a full relaxation of the composite oxide film + metal substrate system to quantify the contribution due to rumpling. In step (iii), a simple DF+U protocol to estimate separately the contribution due to charge compression is discussed, and the difference between the work function of the bare metal slab and a Pauling-like electronegativity (the middle of the band gap) of the free oxide film is used as a descriptor quantity to predict the direction and the magnitude of charge transfer. The present findings shed a clearer light on the physics of the metal/oxide interaction and provide a consistent picture of the phenomenon under consideration. Future research directions include the coupling of an ultrathin oxide-on-metal system with an external electric field, which can provide a further degree of freedom in modulating charge flow at the interface.

■ ASSOCIATED CONTENT

Supporting Information

Behavior of the work function of the NiO/Ag(100) ML system as a function of the value of Hubbard *U* used on the Ni atoms. This material is available free of charge via the Internet at http://pubs.acs.org.

■ AUTHOR INFORMATION

Corresponding Author

*E-mail: alessandro.fortunelli@cnr.it.

Present Address

[∇]Present address: School of Physics, University of Exeter, Exeter EX4 4QL, U.K.

Notes

The authors declare no competing financial interest.

■ ACKNOWLEDGMENTS

This work has been carried out within the framework of the ERC Advanced Grant SEPON. Computational resources within the UT-Ox ISCRA project at the CINECA supercomputing center and technical assistance by Alberto Coduti are gratefully acknowledged.

■ REFERENCES

(1) Surnev, S.; Ramsey, M. G.; Netzer, F. P. *Prog. Surf. Sci.* **2003**, *73*, 117−165.

(2) Chen, M. S.; Goodman, D. W. *J. Phys.: Condens. Matter* **2008**, *20*, 264013.

(3) Freund, H.-J. *Surf. Sci.* **2007**, *601*, 1438−1442.

(4) Wu, Q. H.; Fortunelli, A.; Granozzi, G. *Int. Rev. Phys. Chem.* **2009**, *28*, 517−576.

(5) Schmid, M.; Kresse, G.; Buchsbaum, A.; Napetschnig, E.; Gritschneder, S.; Reichling, M.; Varga, P. *Phys. Rev. Lett.* **2007**, *99*, 196104.

(6) F.;Rizzi, G. A.; Agnoli, S.; Xamena, F. X. L. I.; Papageorgiou, A.; Ostermann, D; Sambi, M.; Finetti, P.; Schierbaum, K.; Granozzi, G. *J. Phys. Chem. B* **2005**, *109*, 24411−24426.

(7) König, T.; Simon, G. H.; Rust, H.-P.; Heyde, M. *J. Phys. Chem. C* **2009**, *113*, 11301−11305.

(8) Ploigt, H. C.; Brun, C.; Pivetta, M.; Patthey, F.; Schneider, W. D. *Phys. Rev. B* **2007**, *76*, 195404.

(9) Magkoev, T. T.; Vladimirov, G. G. *J. Phys.: Condens. Matter* **2001**, *13*, L655−L662.

(10) Krischok, S.; Stracke, P.; Höfft, O.; Kempter, V.; Zhukovskii, Yu. F.; Kotomin, E. A. *Surf. Sci.* **2005**, *600*, 3815−3820.

(11) Rota, A.; Altieri, S.; Valeri, S. *Phys. Rev. B* **2009**, *79*, 161401 and references therein..

(12) Giordano, L.; Pacchioni, G. *Acc. Chem. Res.* **2011**, *44*, 1244−1252 and references therein..

(13) Choi, S. E.; Oh, Y. T.; Ham, H. K.; Kim, T. W; Heo, G. S.; Park, J. W.; Choi, B. H.; Shin, D. C. *Curr. Appl. Phys.* **2011**, *11*, S255−S257.

(14) Jung, J.; Shin, H. J.; Kim, Y.; Kawai, M. *Phys. Rev. B* **2010**, *82*, 085413.

(15) Zhao, W.; Wang, R. Z.; Han, S.; Xue, K.; Wang, H.; Yan, H. *J. Phys. Chem. C* **2010**, *114*, 11584−11587.

(16) Pacchioni, G.; Giordano, L.; Baistrocci, M. *Phys. Rev. Lett.* **2005**, *94*, 226104.

(17) Giordano, L.; Cinquini, F.; Pacchioni, G. *Phys. Rev. B* **2006**, *73*, 145414.

(18) Sterrer, M.; Risse, T.; Heyde, M.; Rust, H. P.; Freund, H. J. *Phys. Rev. Lett.* **2007**, *98*, 206103.

(19) Giordano, L.; Pacchioni, G.; Goniakowski, J.; Nilius, N.; Rienks, E. D. L.; Freund, H. J. *Phys. Rev. B* **2007**, *76*, 075416.

(20) Jerratsch, J. F.; Nilius, N.; Freund, H. J.; Martinez, U; Giordano, L.; Pacchioni, G. *Phys. Rev. B* **2009**, *80*, 245423.

(21) Prada, S.; Martinez, U.; Pacchioni, G. *Phys. Rev. B* **2008**, *78*, 235423.

(22) Goniakowski, J.; Noguera, C. *Phys. Rev. B* **2009**, *79*, 155433.

(23) Giannozzi, P.; Baroni, S.; Bonini, N.; Calandra, M.; Car, R.; Cavazzoni, C.; Ceresoli, D.; Chiarotti, G.; Cococcioni, M.; Dabo, I.; Dal Corso, A.; De Gironcoli, S.; Fabris, S.; Fratesi, G.; Gebauer, R.; Gerstmann, U.; Gougoussis, C.; Kokalj, A.; Lazzeri, M.; Martin-Samos, L.; Marzari, N.; Mauri, F.; Mazzarello, R.; Paolini, S.; Pasquarello, A.; Paulatto, L.; Sbraccia, C.; Scandolo, S.; Sclauzero, G.; Seitsonen, A. P.; Smogunov, A.; Umari, P.; Wentzcovitch, R. M. *J. Phys.: Condens. Matter* **2009**, *21*, 395502.

(24) Dovesi, R.; Orlando, R.; Civalleri, B.; Roetti, C.; Saunders, V. R.; Zicovich-Wilson, C. M. *Z. Kristallogr.* **2005**, *220*, 571−573.

(25) Dovesi, R.; Saunders, V. R.; Roetti, C.; Orlando, R.; Zicovich-Wilson, C. M.; Pascale, F.; Civalleri, B.; Doll, K.; Harrison, N. M.; Bush, I. J.; D'Arco, P.; Llunell, M. *CRYSTAL09 User's Manual*; University of Torino, Torino, Italy, 2009.

(26) Vanderbilt, D. *Phys. Rev. B* **1990**, *41*, 7892−7895.

(27) Perdew, J. P.; Burke, K.; Ernzerhof, M. *Phys. Rev. Lett.* **1996**, *77*, 3865−3868.

(28) Anisimov, V. I.; Zaanen, J.; Andersen, O. K. *Phys. Rev. B* **1991**, *44*, 943−954.

(29) Altieri, S.; Tjeng, L. H.; Voogt, F. C.; Hibma, T.; Sawatzky, G. A. *Phys. Rev. B* **1999**, *59*, R2517−R2520.
(30) Altieri, S.; Finazzi, M.; Hsieh, H. H.; Haverkort, M. W.; Lin, H.-J.; Chen, C. T.; Frabboni, S.; Gazzadi, G. C.; Rota, A.; Valeri, S.; Tjeng, L. H. *Phys. Rev. B* **2009**, *79*, 174431.
(31) Barcaro, G.; Thomas, I. O.; Fortunelli, A. *J. Chem. Phys.* **2010**, *132*, 124703.
(32) Wang, L.; Maxisch, T.; Ceder, G. *Phys. Rev. B* **2006**, *73*, 195107.
(33) Andrae, D.; Haeussermann, U.; Dolg, M.; Stoll, H.; Preuss, H. *Theor. Chim. Acta* **1990**, *77*, 123−141.
(34) www.crystal.unito.it (accessed January 1, 2012).
(35) Becke, A. D. *J. Chem. Phys.* **1993**, *98*, 5648−5652.
(36) Perdew, J. P. *Electronic structure of solids*; Akademie Verlag: Berlin, Germany, 1991.
(37) Casassa, S.; Ferrari, A. M.; Busso, M.; Pisani, C. *J. Phys. Chem. B* **2002**, *106*, 12978−12985.
(38) Moreira, I. P. R; Illas, F.; Martin, R. *Phys. Rev. B* **2002**, *65*, 155102.
(39) Vydrov, O. A.; Heyd, J.; Krukau, A. V.; Scuseria, G. E. *J. Chem. Phys.* **2006**, *125*, 074106.
(40) Doll, K. *Surf. Sci.* **2006**, *600*, L321−L325.
(41) Chelvayohan, M.; Mee, C. H. B. *J. Phys. C: Solid State Phys.* **1982**, *15*, 2305−2312.
(42) Bader, R. F. W. *Chem. Rev.* **1991**, *91*, 893−928.
(43) Created using the Xcrysden code; see: Kokalj, A. *Comput. Mater. Sci.* **2003**, *28*, 155. Code available from http://www.xcrysden.org/ (accessed Jan. 14, 2012).
(44) Weirum, G.; Barcaro, G.; Fortunelli, A.; Weber, F.; Schennach, R.; Surnev, S.; Netzer, F. P. *J. Phys. Chem. C* **2010**, *114*, 15432−15439.
(45) Pauling, L. *The Nature of the Chemical Bond*; Cornell University Press: New York, 1960.
(46) Goniakowski, J.; Noguera, C. *Interface Sci.* **2004**, *12*, 93−103.
(47) Noguera, C. *Physics and chemistry at oxide surfaces*; Cambridge University Press: Cambridge, U.K., 1996.
(48) Jaouen, T.; Jézéquel, G.; Delhaye, G.; Lépine, B.; Turban, P.; Schieffer, P. *Appl. Phys. Lett.* **2010**, *97*, 232104.
(49) Tejedor, C.; Flores, C.; Louis, E. *J. Phys. C* **1977**, *10*, 2163−2178.
(50) Bordier, G.; Noguera, C. *Phys. Rev. B* **1991**, *44*, 6361−6371.
(51) Mönch, W. *Rep. Prog. Phys.* **1990**, *53*, 221−371.
(52) Barcaro, G.; Fortunelli, A.; Granozzi, G. *Phys. Chem. Chem. Phys.* **2008**, *10*, 1876−1882.
(53) Barcaro, G.; Fortunelli., A. *J. Phys. Chem. A* **2009**, *113*, 14860−14866.
(54) Goniakowski, J.; Noguera, C.; Giordano, L.; Pacchioni, G. *Phys. Rev. B* **2009**, *80*, 125403.